# Easy enrichment of graphitic nitrogen to prepare highly catalytic carbons for oxygen reduction reaction

Javier Quílez-Bermejo, Sara Pérez-Rodríguez, Rafael Canevesi, Daniel Torres, Emilia Morallón, Diego Cazorla-Amorós, Alain Celzard, Vanessa Fierro

# Easy enrichment of graphitic nitrogen to prepare highly catalytic carbons for oxygen reduction reaction

Javier Quílez-Bermejo[1,*], Sara Pérez-Rodríguez[1], Rafael Canevesi[1], Daniel Torres[1], Emilia Morallón[2], Diego Cazorla-Amorós[3], Alain Celzard[1], Vanessa Fierro[1,*]

[1] Université de Lorraine, Centre National de la Recherche Scientifique (CNRS), Institut Jean Lamour (IJL), F-88000, Épinal, France.

[2] Departamento de Química Física and Instituto de Materiales, Universidad de Alicante, Ap. 99, 03080, Alicante, Spain

[3] Departamento de Química Inorgánica and Instituto de Materiales, Universidad de Alicante, Ap. 99, 03080, Spain.

* Corresponding author.

E-mail address: vanessa.fierro@univ-lorraine.fr (Vanessa Fierro)

**Abstract**

One of the biggest challenges in producing fuel cells at affordable prices is to synthesize carbon materials selectively doped with graphitic nitrogen, as it is considered the most active nitrogen species for the oxygen reduction reaction (ORR). So far, all strategies focus on the use of nitrogen-containing carbon precursors, which limits the functionalization of commercially available carbon materials. Here, we present a post-functionalization method to boost the catalytic properties of carbon materials for the ORR by selectively enriching activated carbons with nitrogen graphitic species. A commercial high-surface area activated carbon was post-functionalized by a two-step procedure. First, the commercial carbon was mixed with different carbon / urea weight ratios and heated in air at 350 ºC. Then, the functionalized materials were heat-treated at high temperature (from 700 to 1300 ºC) to tailor the amount and distribution of the different nitrogen species in the resulting carbon structure. Nitrogen functionalization using a carbon to urea weight ratio of 1:2 and heat-treatment at 1100 ºC led to highly selective doping in graphitic nitrogen species, which provided the tools to individually asses the catalytic activity of these nitrogen species. In addition, this study presents a low-cost and easily feasible synthesis route to improve the catalytic activity of carbon materials, leading to an onset potential of almost 0.9 V compared to reversible hydrogen electrode for ORR in an alkaline electrolyte. Moreover, this study provides significant evidence for the key role of graphitic nitrogen.

**Highlights**

- An efficient and selective N-functionalization of activated carbons is presented
- This selective post-functionalization does not modify the textural properties
- Carbon materials selectively enriched with graphitic nitrogen were produced
- Graphitic nitrogen appears to be a highly active site for ORR

**Keywords:** oxygen reduction reaction, electrocatalysts, porous carbons, nitrogen, functionalization, graphitic enrichment.

## 1. Introduction

The oxygen reduction reaction (ORR) has a huge impact on the development of many electrochemical devices, such as fuel cells or metal-air batteries [1–4]. This reaction is considered a bottleneck in these technologies due to its sluggish kinetics and large overpotentials [5,6]. The commercial electrodes that are commonly used to catalyze ORR are extremely expensive to make this forefront equipment competitive in comparison with current fossil fuel-based engines [7,8]. The most common commercial ORR electrocatalysts are based on platinum nanoparticles supported on carbon materials [3,7,8]. Platinum is a rare material in nature, which drives the cost of the cathode to unsustainable levels. Moreover, these metal nanoparticles lixiviate and agglomerate under working conditions, reducing the catalytic activity over time [9,10].

Several materials have been presented as attractive alternatives to platinum-based catalysts [5,11,12]. It is worth noting the significant findings in recent years on carbon materials, which have emerged as a promising option to develop low-cost ORR electrodes, given that carbon and carbon precursors are abundant in nature and that carbon-based electrodes are affordable for large-scale implementation [4,13,14].

In general, it is known that the catalytic activity of carbon materials is related to the amount and chemical nature of the active sites [15]. Undoped carbon materials have been shown to be far from the commercial electrocatalysts due to the homogeneous charge distribution along the carbon layers that does not facilitate the chemisorption of dioxygen molecules [16]. Nevertheless, surface area and well-controlled pore size distribution of carbon materials play an important role in the ORR catalysis. Indeed, a large surface area with well-developed microporosity has been shown to be favorable for achieving exceptional ORR activities [17,18].

Despite this, the introduction of defects or heteroatoms, in particular nitrogen (N), is crucial to achieve excellent catalytic properties in carbon-based catalysts [4]. In this sense, some N-doped carbon materials have been shown to catalyze the ORR with almost platinum-like performance [19,20], although the origin of this high catalytic activity is still unclear. Important findings have been made in recent years, leading to a general understanding of the active sites of these carbon-based catalysts; the introduction of nitrogen atoms into the carbon layers results in an electron-withdrawal effect towards the adjacent carbon atoms, creating a positive charge density that facilitates chemisorption of dioxygen molecules and their reduction [21–23]. Although knowledge about the origin of catalytic activity is increasing, still some controversy exists about which N functional groups create the highest activities towards the ORR. Most scientists agree that pyridines and graphitic nitrogen seem to be the most promising species [13,24,25]. Nevertheless, due to the coexistence of different nitrogen species in most carbon materials, the individual evaluation of their catalytic activity is difficult. Recent results obtained with carbon materials selectively doped with graphitic nitrogen show high catalytic activity, close to that for platinum [26,27]. However, N-doped carbon materials that have been obtained with purely graphitic N require complex methodologies and the use of N-containing carbon precursors, making it impossible to extend the synthetic route to other carbon materials. Therefore, post-functionalization methodologies for purely graphitic N enrichment are mandatory in order to selectively introduce graphitic N species into multiple carbon materials while retaining most of the properties of the pristine carbon materials. Graphitic N can further improve the performance of carbon materials not only for ORR electrocatalysts, but also for multiple applications.

In this study, highly efficient metal-free carbon-based catalysts have been synthesized from selective doping with graphitic nitrogen of a well-known commercial activated carbon and using a straightforward post-functionalization methodology. This high-surface area

commercial carbon was doped with urea at different carbon to urea mass ratios, and heat-treated at several temperatures to tune its surface chemistry. Some functionalization treatments led to very efficient catalysts for ORR, approaching platinum-based electrocatalysts. The extensive characterization and electrocatalytic results provided important findings that corroborate the role of graphitic nitrogen in the catalytic activity towards ORR of N-doped carbon materials.

## 2. Materials and methods

### *2.1 Preparation of nitrogen-doped activated carbons*

A commercial activated carbon, MSC30 (Kansai Coke and Chemicals Co., Ltd. Japan), was functionalized using urea as a nitrogen precursor by a two-step procedure. First, MSC30 and urea were physically mixed in mass ratios of 1:1 and 1:2 and subjected to heat treatment in a quartz boat up to 350 ºC for 3 h with a heating rate of 5 ºC $min^{-1}$ in synthetic air (50 mL $min^{-1}$). The resulting samples were cooled to room temperature. The samples were labeled MSC30-U1 and MSC30-U2, according to the carbon to urea weight ratio.

After urea functionalization, MSC30-U1 and MSC30-U2 were heat-treated over a wide range of temperatures, from 700 to 1300 ºC, in order to vary the degree of functionalization and the contribution of the different nitrogen species. The heat treatment was performed in a tubular furnace with a heating rate of 5 ºC $min^{-1}$ (or 2.5 ºC $min^{-1}$ in the case of temperatures above 1100 ºC) under $N_2$ atmosphere (or Ar for temperatures above 1100 ºC). The obtained samples were labeled MSC30-*Y*-*T*, with *Y* being the functionalization process (U1 or U2) and *T* being the temperature of the heat treatment (700, 900, 1100, or 1300 ºC).

### *2.2 Physicochemical characterization*

The mass contents of carbon, hydrogen, oxygen and nitrogen were determined using a Vario EL cube analyzer (Elementar). 10 mg of each sample was introduced into a combustion vessel

and treated at 1700 ºC in a mixed atmosphere of oxygen and helium. The resultant gasses were separated through a chromatographic column and quantified by a thermal conductivity detector with a sensitivity of 40 ppm. In a second separate combustion experiment, the oxygen-containing gases were reduced to CO, from which O quantification was performed. The surface chemistry and oxidation states of the nitrogen functional groups were studied by X-ray photoelectron spectroscopy (XPS), in a VG-Microtech Multilab 3000 spectrometer, with a non-monochromatised Al Kα X-ray source under vacuum. The C1s peak at 284.6 eV was used for binding energy corrections. The deconvolution of the N1s spectra was done by least squares fitting using Gaussian-Lorentzian curves.

The morphology and structure of the heat-treated carbon materials were analyzed using a JEM – ARM 200F Cold FEG transmission electron microscopy (TEM) operating at 200 kV. Prior to the experiments, the carbon powder was dispersed in ethanol and deposited in droplets on a holey carbon grid. The chemical composition was followed using energy-dispersive X-ray spectroscopy (EDX), with a JEOL spectrometer (SDD) in scanning transmission microscopy (STEM) mode. STEM images were obtained in high-angle annular dark field (HAADF) mode.

Raman spectroscopy was performed using a Horiba XploRa Raman apparatus equipped with a 50× long-range objective. The spectra were obtained between 800 and 2000 $cm^{-1}$, using a holographic grating with 1200 lines per mm and a circularly polarized laser of 638 nm, filtered at 10% of its maximum energy to avoid heating of the samples.

To measure the textural properties of the carbon materials, $N_2$ and $H_2$ adsorption isotherms were acquired at -196 ºC, on a 3Flex manometric sorption analyzer (Micromeritics, Atlanta, GA). Prior to adsorption measurements, all samples were outgassed under high vacuum and at 110 ºC for 12h. Pore size distribution (PSD), cumulative pore volume and total surface area ($S_{NLDFT}$) were calculated from the combination of $N_2$ and $H_2$ adsorption isotherms using a

two-dimensional non-local density functional model (2D -NLDFT) available in SAIEUS software (Micromeritics, Atlanta, GA) [28]. $H_2$, instead of $CO_2$, was used to determine pores between 0.3 and 0.7 nm because $H_2$ has a smaller cross-sectional area but also a lower quadrupole moment than $CO_2$. Therefore, $H_2$ is more appropriate to characterize carbons with a high heteroatom content [29], which is the case in the present study. The other textural characteristics were obtained by integration of the PSDs, such as: total pore volume, $V_T$; ultramicropore volume (pore diameter below 0.7 nm), $V_{ult\text{-}\mu icro}$; supermicropore volume (pore diameter between 0.7 and 2 nm), $V_{sup\text{-}\mu icro}$; micropore volume (pore diameter below 2.0 nm), $V_{\mu icro}$; and mesopore volume (pore diameter between 2.0 and 50 nm), $V_{MES}$. The BET area ($A_{BET}$) was calculated by applying the Brunauer-Emmet-Teller theory, using the adequate relative pressure range [30,31].

*2.3 Electrochemical characterization*

The electrochemical ORR tests were performed using a rotating ring-disk electrode (RRDE) in a conventional three-electrode cell on an Autolab PGSTAT302 potentiostat (Metrohm, Netherlands). The RRDE was equipped with a glassy carbon disk (5 mm in diameter) and a platinum ring as the second working electrode. The reference electrode consisted of a reversible hydrogen electrode (RHE) immersed in the working solution and a graphite rod was used as the counter electrode.

The working electrodes for ORR measurements were prepared as follows: 1 mg of carbon-based catalyst was ultrasonically dispersed in 0.25 mL of an aqueous solution of 0.2 wt.% Nafion® and 20 wt.% isopropanol. Then, 33 µL of carbon ink was deposited dropwise on the disk electrode to reach 685 $\mu g \cdot cm^{-2}$ of catalyst loading. Linear sweep voltammetry (LSV) was performed from 1.0 to 0.0 V vs RHE in 0.1 M KOH solution saturated with $O_2$ at a scan rate of 5 $mV \cdot s^{-1}$ at 1600 rpm. Double-layer capacitive effects was compensated from a previous LSV curve in a $N_2$-saturated 0.1 M KOH solution under the same experimental conditions

[32]. The platinum ring was held during the LSV experiments at 1.5 V vs RHE to calculate the $H_2O_2$ yield and the number of electrons transferred during the ORR experiments [33]. The onset potential ($E_{ONSET}$) was determined at a current density of -0.1 $mA \cdot cm^{-2}$ and the half-wave potential ($E_{1/2}$) was calculated as the potential at which the current is equal to half of the diffusion current.

Long-term stability tests were performed by chronoamperometric analysis for the most catalytic sample. The working electrode was fixed at 0.70 V vs RHE for 10 000 s at a rotation speed of 1600 rpm and under continuous oxygen bubbling. The resistance to methanol poisoning was also tested by LSV analysis. LSV curves were obtained using the most catalytic sample before and after addition of methanol. For this experiment, methanol was added into the electrolyte to attain a methanol concentration of 1 M.

## 3. Results and discussion

### *3.1 Physicochemical properties*

A schematic representation of the experimental procedure can be found in Fig. 1a, which recalls what was explained in detail in Section 2.1. This also highlights the sustainability of the process, as no hazardous reagents were used in the synthesis of the N-doped carbon materials. Moreover, urea was used as cheap and abundant nitrogen precursor, which is obtained from ammonia and carbon dioxide. Thus, the proposed synthesis from urea and commercial carbon can be an ideal route to prepare N-doped carbon electrocatalysts while consuming greenhouse gases.

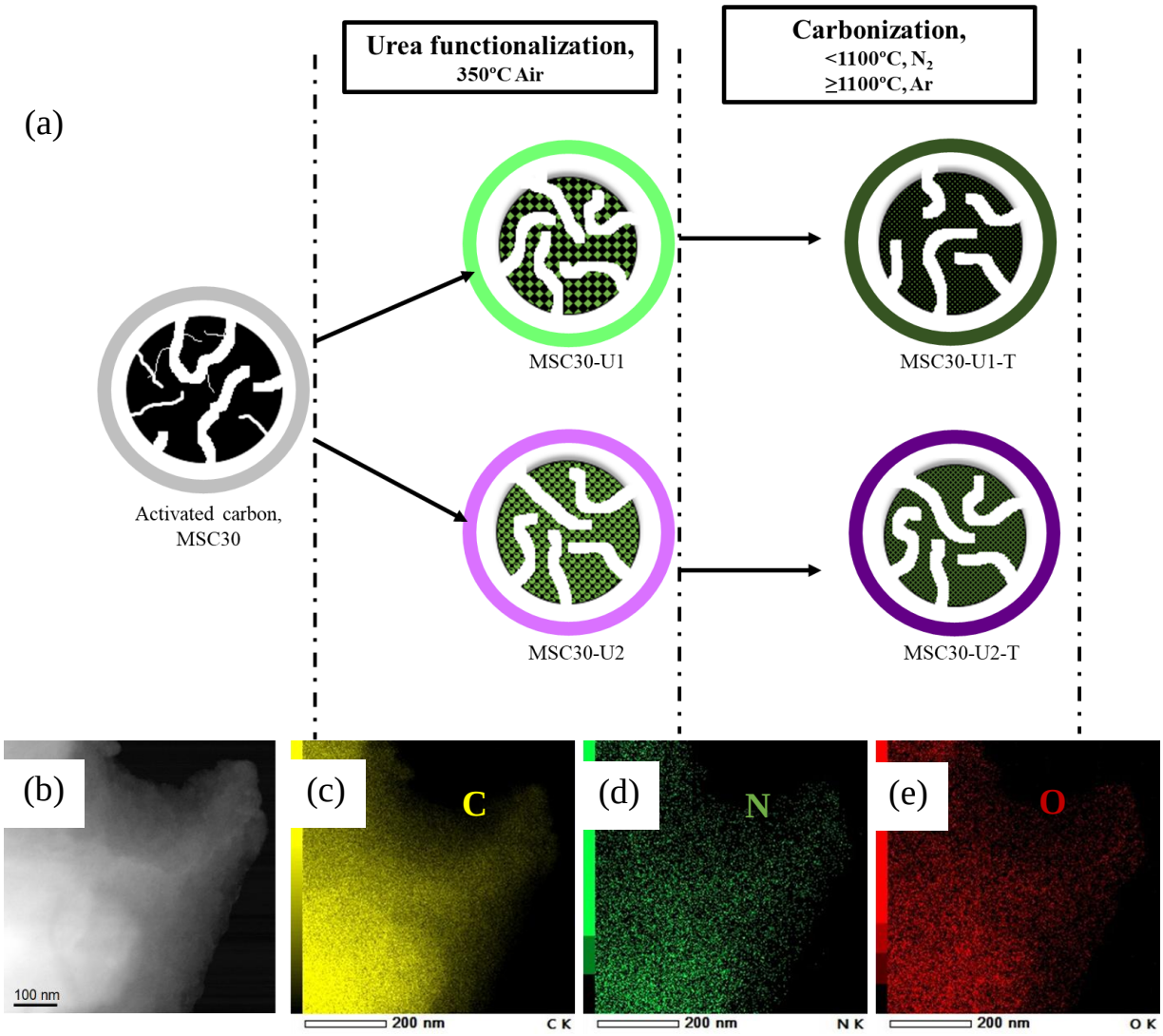


**Fig. 1:** (a) Schematic representation of the experimental procedure. Commercial activated carbon, MSC30, was functionalized with a MSC30 to urea mass ratios of 1:1 or 1:2. These samples were heat-treated from 700 to 1300 ºC in a nitrogen (< 1100 °C) or argon (≥ 1100 °C) atmosphere, with *T* being the temperature of the heat treatment. (b) HAADF image of MSC30-U2-1100 and EDX analyses of (c) carbon, (d) nitrogen and (e) oxygen of the same image.

High-Resolution Transmission Electron Microscopy (HR-TEM) images (Fig. S1-S2) show that the heat-treated samples possess a disordered structure characteristic of activated carbon materials. Moreover, EDX spectroscopy, combined with STEM in HAADF, demonstrates the homogeneous distribution of oxygen and nitrogen species throughout the carbon structure, proving the successful functionalization of the MSC30 samples after heat treatment (Fig. 1b-1e).

The bulk and surface compositions of the carbon materials determined by elemental analysis and XPS are summarized in Tables S1 and S2, respectively. Table S1 also includes the

carbonization yield of the materials. Heat treatment of the pristine MSC30 in the presence of urea at 350 ºC successfully introduced nitrogen into the bulk and at the surface of the activated carbon. Treatment with urea at moderate temperatures often leads to the formation of $C_3N_4$. However, the temperature of 350 ºC does not allow the formation of $C_3N_4$ from urea, as it is known that temperatures around 550 ºC are necessary to produce in-plane ordering [34,35]. According to the literature, HNCO, $NH_3$ and $CO_2$ are the three main volatiles formed during urea functionalization at 350 ºC [36]. Although HNCO (isocyanic acid) is poisonous, it spontaneously reacts with water and hydrolyzes to carbon dioxide and ammonia. Interestingly, MSC30-U2 exhibits twice the surface nitrogen content (8.9 at.%) than its counterpart synthesized with a MSC30 to urea mass ratio of 1:1 (4.4 at.%). The second heat treatment at increasing temperatures from 700 to 1300 ºC resulted in a progressive removal of nitrogen species, which can be explained by thermal decomposition reactions involving urea-based functional groups [37]. A clear influence of the MSC30 to urea mass ratio on the functionalization degree was observed, i.e., the final nitrogen content was considerably higher when MSC30-U2 was used as starting material compared to MSC30-U1. This is best observed by the surface nitrogen content determined by XPS (Table S2). Total removal of surface nitrogen functionalities was obtained at 1100 °C for MSC30-U1, while a higher temperature, 1300 ºC, was required to obtain a carbon material without surface nitrogen using MSC30-U2 as the starting material. These results demonstrate that the nitrogen content of the final material can be easily tuned by controlling the MSC30 to urea mass ratio.

XPS analyses were performed to evaluate the nitrogen speciation in the carbon materials. The full XPS spectra for all samples can be found in Figs. S3-S4. No significant differences were observed in the high-resolution N1s spectra before carbonization (Fig. S5). Low-temperature treatments in the presence of urea lead to the formation of nitrogen groups on the carbon surface instead of nitrogen atoms embedded in the carbon planes [38]. Moreover, the

formation of $C_3N_4$ is ruled out since the N1s spectra are completely different from those of crystalline $C_3N_4$ [34,35,39]. Therefore, the deconvolution of these N1s spectra reveals the presence of amines ($-NH_2$) and imines (=NH) for both MSC30-U1 and MSC30-U2 materials prior to carbonization. The main changes in the surface chemistry of the carbon materials were found after the heat treatments (Fig. 2a and Fig. 2b).

**Fig. 2:** N1s spectra of (a) MSC30-U1, and (b) MSC30-U2 samples after heat treatment at 700, 900, 1100 and 1300 ºC. The blue peak at 398.3 eV represents pyridines, the orange peak at 400.3 eV represents pyrroles or pyridones, and the red peak at 401.2 eV represents graphitic nitrogen species. (c) Contributions of each kind of nitrogen species in the MSC30-U2 samples.

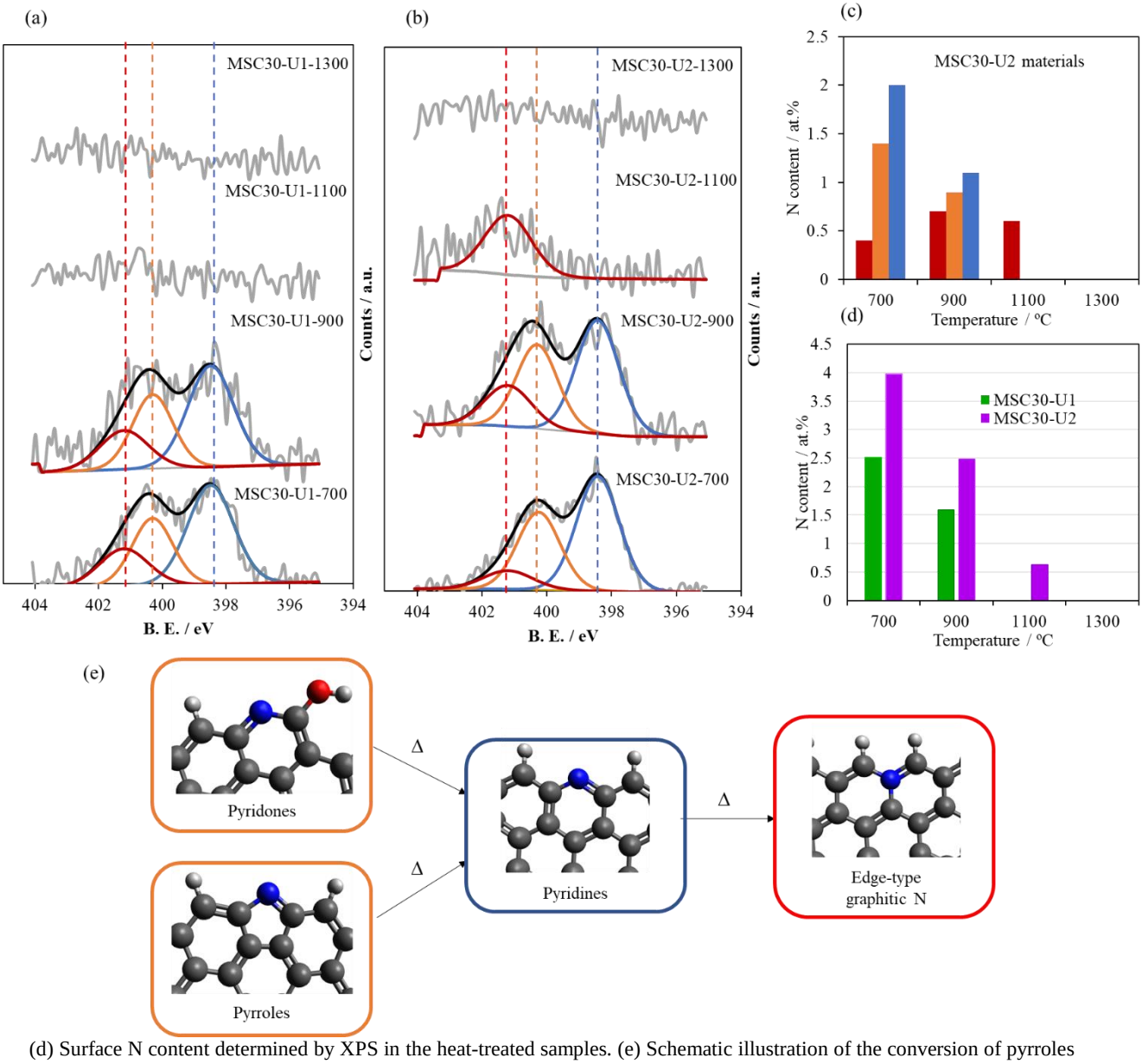


(d) Surface N content determined by XPS in the heat-treated samples. (e) Schematic illustration of the conversion of pyrroles and pyridones into pyridines and the conversion of pyridines into edge-type graphitic nitrogen.

After heat treatment in an inert atmosphere, the N1s spectra of the resulting nitrogen-doped carbons were deconvoluted into three groups according to the literature [27,40,41]: pyridines at 398.3 eV (blue peak), pyrroles and/or pyridones at 400.3 eV (orange peak), and graphitic nitrogen groups (i.e., quaternary nitrogen) at 401.2 eV (red peak). Amines and imines are converted into heterocyclic functionalities at such high temperatures [41]. Fig. 2a-b show that the pyrolysis temperature significantly influences the N1s profiles, and consequently, the relative contribution of nitrogen-containing species (see Table S2). Activated carbons treated at the lowest temperature, 700 °C, showed three peaks in the N1s spectrum, which is indicative of a mix of pyridines, pyrroles/pyridones and graphitic N species. Pyridines are the main contribution (around 50%) at 700 ºC, followed by pyrroles/pyridones (≈ 30%) and graphitic-N functionalities (≈ 20%). With increasing temperature, the contribution of pyridines decreases while an increase of graphitic nitrogen is observed, especially for MSC30-U2-1100, in which all nitrogen is in the form of graphitic species (for MSC30-U1-1100, no nitrogen was detected by XPS at this temperature). This is easily observed in the peak quantification, which is summarized for sample MSC30-U2 in Fig. 2c. The gradual elimination of nitrogen functional groups with increasing temperature is evident in Fig. 2d. No nitrogen content is detected for MSC30-U1-1100, while MSC30-U2-1100 shows an N contribution of 0.6 at.%.

According to the literature, the changes in the N1s profiles are explained by: (i) the greater thermal stability of graphitic nitrogen, and (ii) local changes in the carbon structure, in which pyridine and pyrrole species are transformed into graphitic nitrogen species by condensation reactions at high temperature [41,42]. The increase in total graphitic N content, from 0.4 at.% in MSC30-U2-700 to 0.6 at.% in MSC30-U2-1100 can only be explained through the conversion of pyridines and pyrrole/pyridone species into graphitic nitrogen groups. The main feature of this conversion is that it proceeds in the edges of the carbon layers, leading to the

formation of edge-type graphitic species, whereas the most common location of graphitic species is the basal plane. Pels et al. proposed that pyridones and pyrrolic N species tend to convert to pyridine species at temperatures above 600 ºC through the loss of oxygen from pyridones and the expansion of pyrrole rings; however, such pyridines are also converted into edge-type graphitic nitrogen species if high temperature treatments are used (Figure 2e) [41]. This conversion is especially noteworthy since edge-type graphitic nitrogen groups are proposed as the highest ORR catalytic species in N-doped carbon materials [4]. It also worth mentioning that the surface nitrogen species were completely removed from the carbon surface at 1300 ºC, leading to an undoped (or weakly doped) carbon material. These results confirm the selective enrichment of the porous carbon material with graphitic nitrogen species after the 1100 ºC heat treatment of MSC30-U2.

Raman spectroscopy was performed to study the structural order of the heat-treated carbon materials. Figure S6 shows the Raman spectra for the MSC30-U2_T samples. The $I_D/I_G$ ratio shows a slight variation with heat treatment temperature, indicating that the structural order of carbon materials is progressively changed by the heat treatment. This change is gradual and moderate below 900 ºC, but becomes significant at temperatures above 1100 ºC, for which a clear narrowing of the D and G bands is observed. Nevertheless, these spectra remain typically those of highly disordered and non-graphitizable carbons.

The textural properties of the N-doped and the pristine carbon materials were evaluated using $N_2$ and $H_2$ adsorption isotherms, and the results obtained are gathered in Table 1. $H_2$ adsorption isotherms were performed to characterize the pore size distribution down to 0.3 nm due to smaller cross-section and lower quadrupole moment. Fig. S7 shows the $N_2$ and $H_2$ adsorption isotherms and Fig. S8 shows the cumulative pore volumes calculated by 2D-NLDFT. The $N_2$ adsorption isotherms show that after the functionalization process, part of the porosity of the pristine MSC30 is blocked by the surface groups that hinder the access of the

adsorbate to the micropores. Once the heat treatment is applied at low temperature, 700 ºC, these nitrogen groups lead to the production of heterocyclic nitrogen species in the carbon material, which release part of the blocked porosity and, therefore, increase the surface area. If the highest temperature is used during the heat treatment (i.e., 1300 ºC), a slight loss of surface area is observed due to pore constriction. Both of these effects can be observed in some of the textural properties shown in Table 1 (e.g. $A_{BET}$, $S_{NLDFT}$ and $V_{\mu icro}$) as well as in the adsorption isotherms (Fig. S7) and the cumulative volume plot (Fig. S8). Fig. S8 shows that most of the pore volume of the pristine MSC30 is in the microporosity range, i.e., corresponding to pores below 2 nm, and which is maintained after urea functionalization and subsequent heat treatments. Similar profiles were found for all materials. Nevertheless, the developed textural properties of MSC30 are still present after functionalization and heat treatments.

**Table 1:** Textural properties of the nitrogen-doped carbon materials obtained from $N_2$ and $H_2$ adsorption isotherms. $N_2$ adsorption isotherms were used to calculate $A_{BET}$, and the combination of $N_2$ and $H_2$ adsorption isotherms were used to calculate all other parameters.

| Sample | Textural Properties | | | | | | |
|---|---|---|---|---|---|---|---|
| | $A_{BET}$ [$m^2/g$] | $V_T$ [$cm^3/g$] | $V_{MES}$ [$cm^3/g$] | $V_{\mu icro}$ [$cm^3/g$] | $V_{sup\text{-}\mu icro}$ [$cm^3/g$] | $V_{ult\text{-}\mu icro}$ [$cm^3/g$] | $S_{NLDFT}$ [$m^2/g$] |
| **MSC30** | 3200 | 1.64 | 0.66 | 0.98 | 0.88 | 0.11 | 2500 |
| **MSC30-U1** | 2660 | 1.31 | 0.50 | 0.81 | 0.74 | 0.06 | 2057 |
| **MSC30-U1_700** | 2780 | 1.37 | 0.49 | 0.84 | 0.78 | 0.06 | 2060 |
| **MSC30-U1_900** | 2740 | 1.34 | 0.50 | 0.88 | 0.77 | 0.11 | 2220 |
| **MSC30-U1_1100** | 2870 | 1.47 | 0.57 | 0.90 | 0.72 | 0.18 | 2370 |
| **MSC30-U1_1300** | 2420 | 1.30 | 0.52 | 0.77 | 0.59 | 0.18 | 2200 |
| **MSC30-U2** | 2230 | 1.12 | 0.37 | 0.76 | 0.56 | 0.19 | 2030 |
| **MSC30-U2_700** | 2480 | 1.22 | 0.40 | 0.83 | 0.64 | 0.18 | 2140 |
| **MSC30-U2_900** | 2380 | 1.17 | 0.38 | 0.80 | 0.66 | 0.14 | 2010 |
| **MSC30-U2_1100** | 2560 | 1.27 | 0.47 | 0.81 | 0.67 | 0.14 | 2040 |
| **MSC30-U2_1300** | 2150 | 1.17 | 0.47 | 0.70 | 0.50 | 0.20 | 2040 |

*3.2 Electrocatalytic activity*

Figures 3a-b show the LSV curves before and after the heat treatment of the MSC30-U1 and MSC30-U2 samples, respectively. The MSC30 material was also included for comparison

(dashed lines). A summary of the ORR electrocatalytic parameters is given in Table S3. Heat treatment of MSC30 in the presence of urea at 350 ºC did not enhance the catalytic activity towards ORR, neither from the point of view of the onset potential, $E_{ONSET}$, nor from the point of view of the limiting current density, *j*, as shown by the LSV curves of the MSC30-U1 and MSC30-U2 materials. This fact might be related to the chemical nature of the nitrogen species in these samples, containing mainly amines and imines (see Supporting Information, Fig. S5). These nitrogen species have been shown to be inactive for oxygen reduction [4]. Moreover, the catalytic activity seems to be slightly reduced due to pore blocking by the non-active nitrogen functional groups, in good agreement with the results obtained by $N_2$ and $H_2$ physisorption.

A clear effect of pyrolysis temperature on electrochemical performance was observed. In the case of MSC30-U1 samples, the thermal treatment at 700 ºC improves the limiting current density, compared to pristine MSC30 (dashed line). This increase in catalytic activity continues up to 900 ºC, where the optimum catalytic activity appears to be achieved (onset potential of 0.85 V, $E_{1/2}$ = 0.74 V, and limiting current density of -5.5 mA $cm^{-2}$). At temperatures above 900 ºC, the higher the annealing temperature, the lower the current density, with values of -4.9 and -3.5 mA $cm^{-2}$ for MSC30-U1-1100 and MSC30-U1-1300, respectively. Moreover, a shift to more negative values was observed in the onset potential with increasing temperature. This lower electrochemical performance for the samples treated at 1100 and 1300 ºC is explained by the total removal of surface nitrogen, as evidenced by XPS. These results demonstrate that nitrogen species are necessary to promote highly efficient ORR. For the analogous MSC30-U2 materials (Fig. 3b), the trend is slightly different since the N content is higher at all temperatures. For these materials, the same improvement in catalytic activity is observed up to 900ºC. However, unlike MSC30-U1, there is still an improvement in catalytic activity for the materials heat-treated at 1100 °C. This is noteworthy

since the N content of MSC30-U2-1100 (c.a. 0.6 at.%) seems to be high enough to reduce the dioxygen molecules.

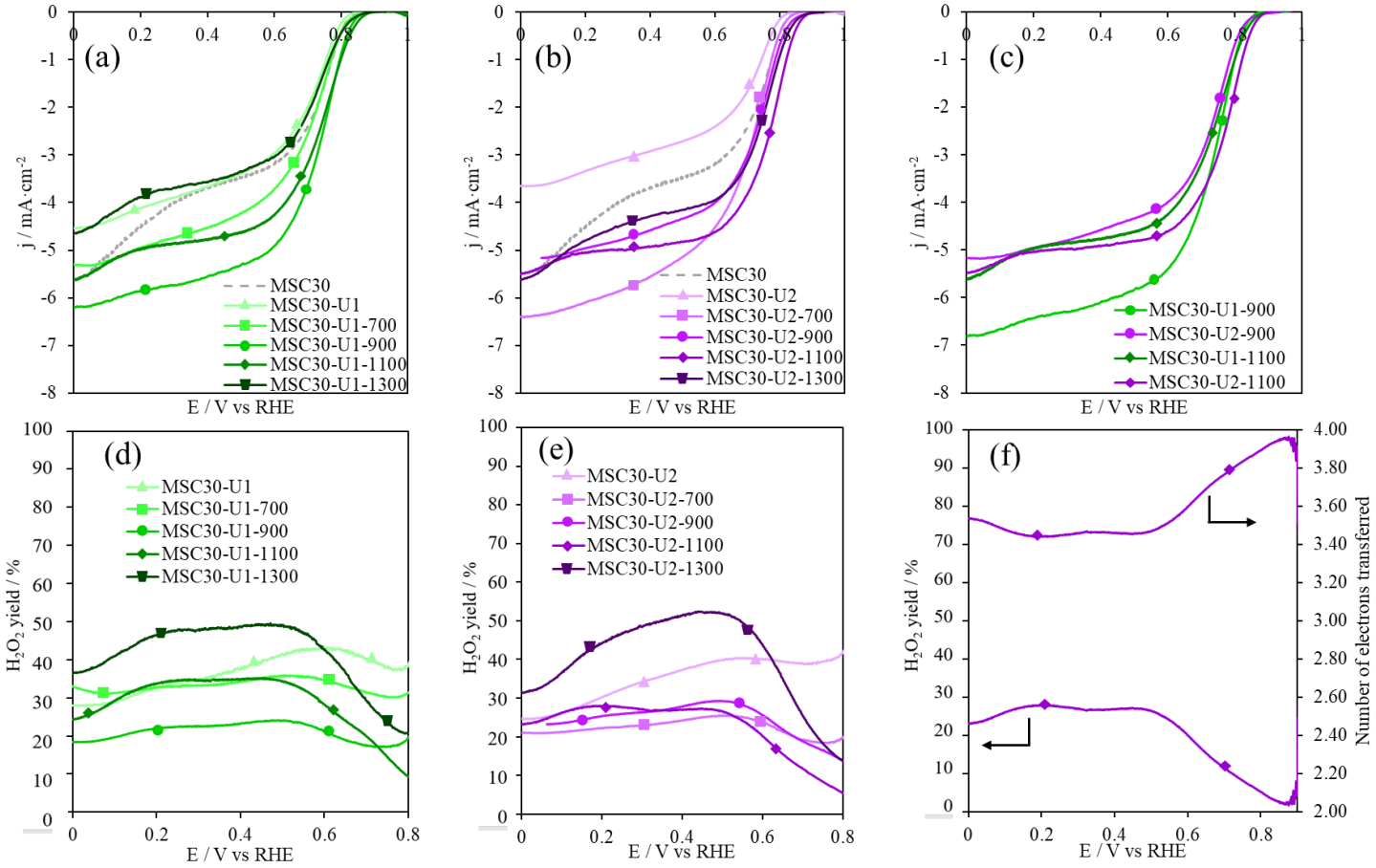


**Fig. 3:** LSV curves for N-doped carbon materials obtained after heat treatment of (a) MSC30-U1, and (b) MSC30-U2 in 0.1 M KOH solution saturated with $O_2$ at a scan rate of 5 $mV \cdot s^{-1}$. (c) Comparison of ORR curves for the most active materials in the same conditions as in (a) and (b). (d,e) $H_2O_2$ yield calculated from the current of the platinum ring during ORR experiments. (f) $H_2O_2$ yield and number of electrons transferred for MSC30-U2-1100.

These results show that the initial nitrogen content of the as-synthesized MSC30-U1 and MSC30-U2 plays an important role on the catalytic activity of the resulting samples annealed at different temperatures. The electrochemical responses for ORR of the most promising materials are compared in Fig. 3c. MSC30-U2-1100 exhibits the highest catalytic performance for ORR with an onset potential of about 0.88 V, $E_{1/2}$ of 0.78 V and 3.8 number of electrons transferred (see Table S3). The presence of this optimized electrocatalytic behavior for oxygen reduction seems to be related to the specific surface chemistry of this

sample, containing only graphitic-N species. The following most catalytic samples are MSC30-U1-1100 and MSC30-U1-900 with a significant decrease in $E_{ONSET}$ to 0.85 V, $E_{1/2}$ to 0.74 V and number of electrons transferred to 3.6. The samples obtained from MSC30-U1 show lower onset potentials probably due to: i) the lower temperature used during the heat treatment in the case of MSC30-U1-900, which does not allow the complete enrichment in graphitic nitrogen species, or ii) due to the lack of surface nitrogen species at temperatures above 1100 ºC (see the N1s spectrum in Fig. 2a). These results evidence that the most positive onset potentials were obtained for the sample with low nitrogen content (0.6 at.%), but in the form of exclusively graphitic nitrogen species.

The hydrogen peroxide yield, which is indicative of ORR mechanisms, is shown in Fig. 3d and 3e. Interestingly, all materials show low $H_2O_2$ yield at higher potentials, meaning that the number of electrons transferred is close to 4 in the useful potential range (0.6-1.0 V vs. RHE), a crucial parameter for the energy density of fuel cell stations. Among all the materials, those prepared using MSC30-U2 were the ones that showed lower $H_2O_2$ yield and, consequently, higher number of electrons transferred during ORR, especially the material treated at 1100 ºC. Fig. 3f shows the number of electrons transferred and hydrogen peroxide yield for the most catalytic sample, MSC30-U2-1100, across the potential range. In addition, a minimum $H_2O_2$ yield is observed, about 25%, and the number of electrons transferred remains constant, 3.5, at the less positive potentials. Therefore, the highly porous and graphitic nitrogen-enriched carbon material, obtained by urea functionalization and heat treatment at 1100 ºC, was found to be a highly competitive catalyst for ORR with high selectivity towards the 4-electron pathway.

To support the role of graphitic N species in the catalytic activity of the MSC30 samples, we added two materials for comparison purposes in Fig. 4a. The first material is MSC30-1100, i.e., the sample MSC30 treated at 1100 ºC, to ensure that the enhancement of catalytic activity

was not related to an increase in structural order due to heat treatment of MSC30. The second material is Pt/C, i.e., the commercial platinum-based catalyst. Fig. 4a-b reveal that the highly efficient 4-electron ORR catalysis of MSC30-U2-1100 is related to the graphitic nitrogen species since the sample treated without nitrogen functionalization shows significantly lower catalytic activity. This finding further confirms that selective graphitic enrichment by simple N doping with urea and high-temperature treatment is an efficient and low-cost method to produce excellent metal-free N-doped carbon catalysts for ORR. Graphitic nitrogen species indeed modify the electron density of the adjacent carbon atoms, promoting ORR, as already concluded by theoretical and experimental studies [22,26,42–44].

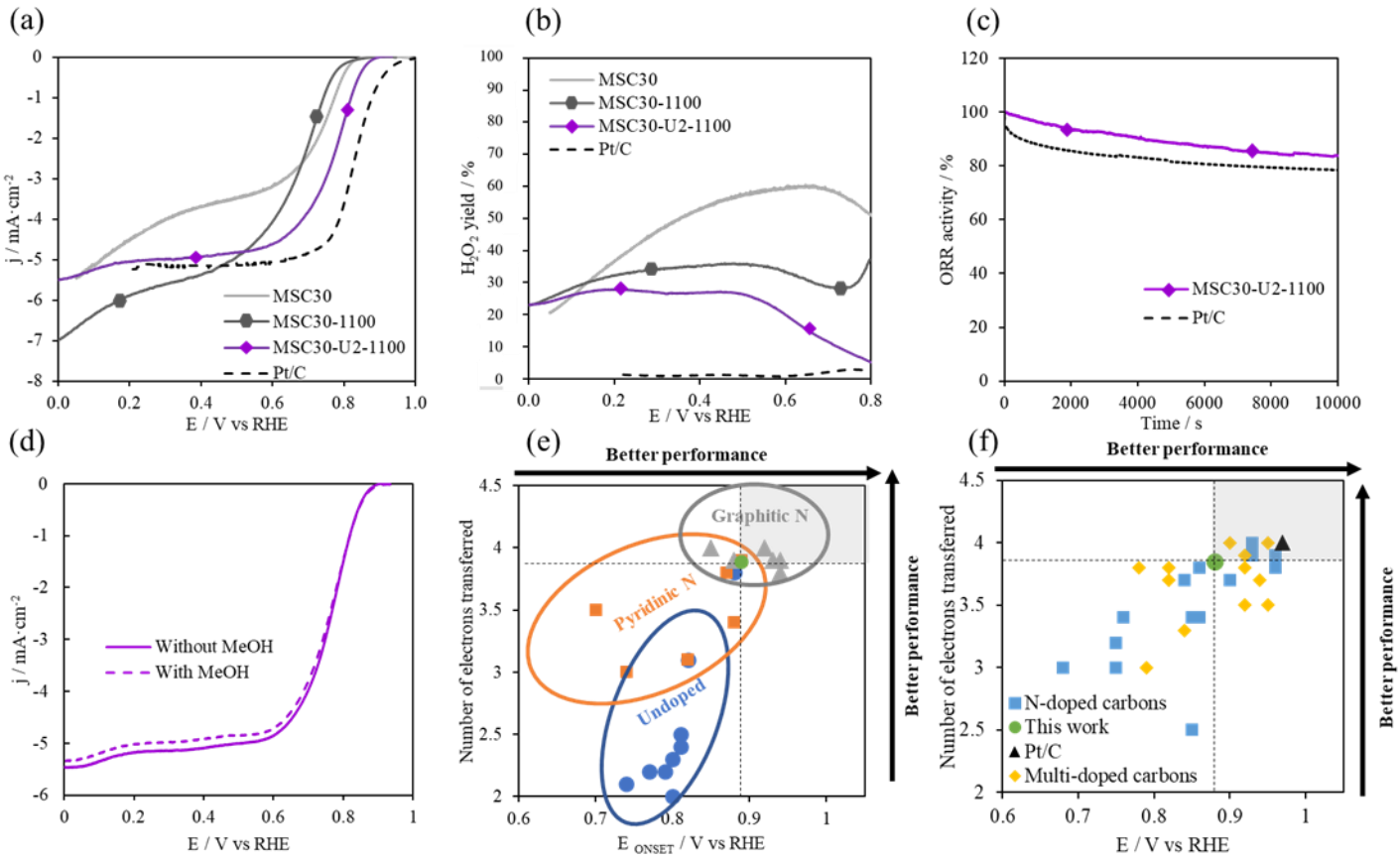


**Fig. 4:** (a) LSV curves, and (b) $H_2O_2$ yield of pristine MSC30, MSC30-1100, and MSC30-U2-1100 in an $O_2$-saturated 0.1 M KOH solution at a scan rate of 5 $mV \cdot s^{-1}$. A 20 wt.% Pt/C catalyst has been included in these figures following the same procedure. (c) Chronoamperometric analysis of MSC30-U2-1100 and Pt/C catalyst at 0.70 V vs RHE in an $O_2$-saturated 0.1 M KOH solution. (d) LSV curves of sample MSC30-U2-1100 before and after the addition of 1 M methanol into an $O_2$-saturated 0.1 M KOH solution at a scan rate of 5 $mV \cdot s^{-1}$. (e) Bibliographic search of metal-free carbon materials with the majority of nitrogen in the form of graphitic or pyridinic N; undoped carbon materials were included for comparison. (f) Bibliographic search of the latest published metal-free carbon-based catalysts towards ORR, including the commercial Pt/C catalysts for comparison; the data were obtained from [17,18,20,23,26,45-80].

Moreover, in order to verify these excellent catalytic properties, stability tests were performed for MSC30-U2-1100 and the commercial Pt-based catalyst. One of the main characteristics of carbon-based catalysts, compared to Pt-based catalyst, is their higher stability towards ORR, as shown in Fig. 4c. After 10 000 s of operation, MSC30-U2-1100 showed outstanding retention of Faradaic current towards ORR, 84 %, which is more stable than the commercial Pt-based catalyst showing only 78 % retention. Most of the activity loss of the Pt-based catalyst occur during the first 1,000 seconds, while MSC30-U2-1100 shows a gradual and slow loss of catalytic activity. Moreover, the Pt-based catalyst also shows important limitations towards MeOH poisoning, making it useless for MeOH-based fuel cells. The

MeOH poisoning test for the commercial Pt-based catalyst was performed (Fig. S9). Methanol was added to the electrolyte to reach a concentration of 1 M, and the ORR experiments were recorded before and after MeOH addition. Fig. S9 shows that MeOH oxidation prevails over ORR when using Pt-based catalyst. At the same time, carbon materials, and in particular MSC30-U2-1100, are catalysts that show excellent tolerance to MeOH poisoning. Fig. 4d shows the LSV curves of MSC30-U2-1100 before and after methanol addition. The catalytic performance of MSC30-U2-1100 showed no differences in $E_{ONSET}$ or limiting current density under the action of methanol, supporting the strong resistance of the graphitic N-enriched carbon material to methanol poisoning.

*3.3 Comparison with the literature*

The paramount role of graphitic N was confirmed by a comparative analysis of different published carbon-based catalysts for the oxygen reduction reaction (ORR) in alkaline electrolyte. Fig. 4e and Table S4 show a detailed literature search of N-doped carbon materials with the majority of the nitrogen (> 50 at.%) in the form of graphitic or pyridinic N. As observed, metal-free carbon materials with pyridines as the main type of nitrogen show better catalytic activity compared to undoped carbon materials. The undoped carbon catalysts show a sluggish ORR activity with a 2-electron mechanism, while pyridine-based carbon materials show the reduction of oxygen molecules through an intermediate number of electrons transferred but a similar $E_{ONSET}$. However, the carbon materials with the majority of the nitrogen as graphitic species show the best catalytic performance for ORR in the N-doped carbon materials, with $E_{ONSET}$ around 0.9 V vs RHE and a number of electrons transferred close to 4. This confirms that graphitic N appears to be the most promising nitrogen species to boost the ORR catalytic activity of N-doped carbon materials and that very good ORR catalysts can be obtained by selectively enriching activated carbons with graphitic N, as presented in this study. Graphitic N, especially that located at the edges of the carbon layers,

produces a dissociative ORR mechanism through bridging (C-O-O-C) bonding modes, leading to the chemisorption of the two oxygen atoms from dioxygen molecules and, consequently, to O-O bond cleavage and a highly selective 4-electron pathway [26]. At the same time, pyridine N and undoped carbons chemisorb oxygen molecules through a terminal (C-O-O) bonding mode, leading to an associative mechanism in which the 2-electron pathway predominates.

Finally, Fig. 4f and Table S5 show the best performance of metal-free carbon-based catalysts in the recent literature. The green circle of this figure reflects the catalytic behavior of the MSC30-U2-1100 material. As can be seen, despite the superb ORR performance of this sample, there are carbon-based materials that still exhibit superior catalytic activities. However, it is important to note that these high performances were achieved by doping with multiple heteroatoms, using expensive reagents, such as graphene, or tedious and complex methodologies. Moreover, all these highly catalytic carbons were obtained from N-containing precursors, which make impossible to control the textural properties of the resulting materials. In contrast, this study proposed a selective and green post-functionalization route to obtain highly catalytic carbons without disturbing significantly the textural properties of the pristine materials, making it a promising synthesis method not only for preparing highly catalytic carbons for ORR, but also for improving the properties of carbon materials in multiple applications.

## 4. Conclusions

Highly porous and graphitic N-enriched carbon materials were prepared by nitrogen doping with urea of a commercial activated carbon material, MSC30, using a simple post-functionalization method. Urea and MSC30 were mixed and heat-treated to obtain N-doped carbon materials with different nitrogen contents and functional groups distributions. Since the heat treatment had no significant effect on the textural properties, the functionalized

carbon materials thus prepared corroborated the key role of graphitic nitrogen in the successful catalysis of the oxygen reduction reaction (ORR). Moreover, these materials showed great potential in terms of catalytic activity ($E_{ONSET}$ = 0.88 V vs RHE; $H_2O_2$ selectivity < 20%; $j$ = -5.0 mA·cm$^{-2}$), exhibiting catalytic performance similar to that of leading metal-free catalysts and even commercial Pt-based electrocatalysts. Furthermore, this study provided an efficient and low-cost method to produce graphitic N-enriched carbon with excellent catalytic activity for ORR, high stability and resistance to methanol poisoning while retaining most of the textural properties intact.

**Acknowledgements:** The French research team thanks ANR-15-IDEX-04-LUE and the TALiSMAN project (2019-000215), financed by the European Regional Development Fund (ERDF). The authors from UA thank MICINN and ERDF (project RTI2018-095291-B-I00) for financial support.

## References


[1] Y.J. Wang, H. Fan, A. Ignaszak, L. Zhang, S. Shao, D.P. Wilkinson, J. Zhang, Compositing doped-carbon with metals, non-metals, metal oxides, metal nitrides and other materials to form bifunctional electrocatalysts to enhance metal-air battery oxygen reduction and evolution reactions, Chem. Eng. J. 348 (2018) 416–437.

[2] M. Li, X. Bi, R. Wang, Y. Li, G. Jiang, L. Li, C. Zhong, Z. Chen, J. Lu, Relating Catalysis between Fuel Cell and Metal-Air Batteries, Matter. 2 (2020) 32–49.

[3] A. Morozan, B. Jousselme, S. Palacin, Low-platinum and platinum-free catalysts for the oxygen reduction reaction at fuel cell cathodes, Energy Environ. Sci. 4 (2011) 1238–1254.

[4] J. Quílez-Bermejo, E. Morallón, D. Cazorla-Amorós, Metal-free heteroatom-doped carbon-based catalysts for ORR. A critical assessment about the role of heteroatoms, Carbon N. Y. 165 (2020) 434–454.

[5] P. Lang, N. Yuan, Q. Jiang, Y. Zhang, J. Tang, Recent Advances and Prospects of Metal-Based Catalysts for Oxygen Reduction Reaction, Energy Technol. 8 (2020) 1900984.

[6] H.A. Gasteiger, S.S. Kocha, B. Sompalli, F.T. Wagner, Activity benchmarks and requirements for Pt, Pt-alloy, and non-Pt oxygen reduction catalysts for PEMFCs, Appl. Catal. B Environ. 56 (2005) 9–35.

[7] C. Sealy, The problem with platinum, Mater. Today. 11 (2008) 65–68.

[8] L. Dai, Y. Xue, L. Qu, H.-J. Choi, J.-B. Baek, Metal-Free Catalysts for Oxygen Reduction Reaction, Chem. Rev. 115 (2015) 4823–4892.

[9] S. Ohyagi, T. Matsuda, Y. Iseki, T. Sasaki, C. Kaito, Effects of operating conditions on

durability of polymer electrolyte membrane fuel cell Pt cathode catalyst layer, J. Power Sources. 196 (2011) 3743–3749.

[10] R.J.B. M. Winter, What are batteries, fuel cells, and supercapacitors?, Chem. Rev. 104 (2004) 4245–4269.

[11] X. Zhou, J. Qiao, L. Yang, J. Zhang, A review of graphene-based nanostructural materials for both catalyst supports and metal-free catalysts in PEM fuel cell oxygen reduction reactions, Adv. Energy Mater. 4 (2014) 1301523.

[12] Z.L. Y. Xue, S. Sun, Q. Wang, Z. Dong, Transition metal oxide-based oxygen reduction reaction electrocatalysts for energy conversion systems with aqueous electrolytes, J. Mater. Chem. A. 6 (2018) 10596–10626.

[13] K.H. Wu, D.W. Wang, D.S. Su, I.R. Gentle, A Discussion on the Activity Origin in Metal-Free Nitrogen-Doped Carbons for Oxygen Reduction Reaction and their Mechanisms, ChemSusChem. 8 (2015) 2772–2788.

[14] M. Seredych, A. Szczurek, V. Fierro, A. Celzard, T.J. Bandosz, Electrochemical Reduction of Oxygen on Hydrophobic Ultramicroporous PolyHIPE Carbon, ACS Catal. 6 (2016) 5618–5628.

[15] Y. Ji, H. Dong, C. Liu, Y. Li, The progress of metal-free catalysts for the oxygen reduction reaction based on theoretical simulations, J. Mater. Chem. A. 6 (2018) 13489–13508.

[16] Y. Zheng, Y. Jiao, M. Jaroniec, Y. Jin, S.Z. Qiao, Nanostructured metal-free electrochemical catalysts for highly efficient oxygen reduction, Small. 8 (2012) 3550–3566.

[17] L. Yang, J. Shui, L. Du, Y. Shao, J. Liu, L. Dai, Z. Hu, Carbon-Based Metal-Free ORR

Electrocatalysts for Fuel Cells : Past, Present, and Future, Adv. Mater. 31 (2019) 1804799.

[18] A. Gabe, R. Ruiz-Rosas, C. González-Gaitán, E. Morallón, D. Cazorla-Amorós, Modeling of oxygen reduction reaction in porous carbon materials in alkaline medium. Effect of microporosity, J. Power Sources. 412 (2019) 451–464.

[19] K. Gong, F. Du, Z. Xia, M. Durstock, L. Dai, Nitrogen-doped carbon nanotube arrays with high electrocatalytic activity for oxygen reduction, Science (80-. ). 323 (2009) 760–764.

[20] J. Quílez-Bermejo, E. Morallón, D. Cazorla-Amóros, Oxygen reduction catalysis of N-doped carbons prepared via heat treatment of polyaniline at over 1100$^{o}$C, Chem. Commun. 54 (2018) 4441–4444.

[21] J.D. Wiggins-Camacho, K.J. Stevenson, Mechanistic Discussion of the Oxygen Reduction Reaction at Nitrogen-Doped Carbon Nanotubes, J. Phys. Chem. B. 115 (2011) 20002–20010.

[22] J. Quílez-Bermejo, K. Strutynski, M. Melle-Franco, E. Morallón, D. Cazorla-Amorós, On the origin of the effect of pH in ORR for non-doped and edge-type quaternary N-doped metal-free carbon-based catalysts, ACS Appl. Mater. Interfaces. 12 (2020) 54815–54823.

[23] S. Maldonado, K.J. Stevenson, Influence of nitrogen doping on oxygen reduction electrocatalysis at carbon nanofiber electrodes, J. Phys. Chem. B. 109 (2005) 4707–4716.

[24] S.K. Singh, K. Takeyasu, J. Nakamura, Active Sites and Mechanism of Oxygen Reduction Reaction Electrocatalysis on Nitrogen-Doped Carbon Materials, Adv. Mater.

31 (2019) 1804297.

[25] J. Liu, P. Song, Z. Ning, W. Xu, Recent Advances in Heteroatom-Doped Metal-Free Electrocatalysts for Highly Efficient Oxygen Reduction Reaction, Electrocatalysis. 6 (2015) 132–147.

[26] J. Quílez-Bermejo, M. Melle-Franco, E. San-Fabián, E. Morallón, D. Cazorla-Amorós, Towards understanding the active sites for the ORR in N-doped carbon materials through fine-tuning of nitrogen functionalities: an experimental and computational approach, J. Mater. Chem. A. 7 (2019) 24239–24250.

[27] J. Quílez-Bermejo, E. Morallón, D. Cazorla-Amorós, Polyaniline-derived N-doped Ordered Mesoporous Carbon Thin Films: Efficient Catalysts towards Oxygen Reduction Reaction, Polymers (Basel). 12 (2020) 2382.

[28] J. Jagiello, J.P. Olivier, Carbon slit pore model incorporating surface energetical heterogeneity and geometrical corrugation, Adsorption. 19 (2013) 777–783.

[29] J. Jagiello, J. Kenvin, C.O. Ania, J.B. Parra, A. Celzard, V. Fierro, Exploiting the adsorption of simple gases O2 and H2 with minimal quadrupole moments for the dual gas characterization of nanoporous carbons using 2D-NLDFT models, Carbon N. Y. 160 (2020) 164–175.

[30] J. Rouquerol, P. Llewellyn, F. Rouquerol, Is the BET equation applicable to microporous adsorbents?, Stud. Surf. Sci. Catal. 160 (2007) 49–56.

[31] M. Thommes, K. Kaneko, A. V Neimark, J.P. Olivier, F. Rodriguez-Reinoso, J. Rouquerol, K.S.W. Sing, Physisorption of gases , with special reference to the evaluation of surface area and pore size distribution (IUPAC Technical Report), Pure Appl. Chem. 87 (2015) 1051–1069.

[32] L. Bouleau, S. Pérez-Rodríguez, J. Quílez-Bermejo, M.T. Izquierdo, F. Xu, V. Fierro, A. Celzard, Best practices for ORR performance evaluation of metal-free porous carbon electrocatalysts, Carbon N. Y. 189 (2022) 349–361.

[33] C. Du, Y. Sun, T. Shen, G. Yin, J. Zhang, Applications of RDE and RRDE Methods in Oxygen Reduction Reaction, in: Rotating Electrode Methods Oxyg. Reduct. Electrocatal., 2014.

[34] L.T.M. Oanh, L.T. Hang, N.D. Lai, N.T. Phuong, D. V. Thang, N.M. Hung, D.D. Bich, N.V. Minh, Influence of annealing temperature on physical properties and photocatalytic ability of g-C3N4 nanosheets synthesized through urea polymerization in Ar atmosphere, Phys. B Condens. Matter. 532 (2018) 48–53.

[35] J. Liu, T. Zhang, Z. Wang, G. Dawson, W. Chen, Simple pyrolysis of urea into graphitic carbon nitride with recyclable adsorption and photocatalytic activity, J. Mater. Chem. 21 (2011) 14398–14401.

[36] W. Yang, L. Jia, P. Wu, H. Zhai, J. He, C. Liu, W. Jiang, Effect of thermal program on structure–activity relationship of g-C3N4 prepared by urea pyrolysis and its application for controllable production of g-C3N4, J. Solid State Chem. 304 (2021) 122545.

[37] L. Shi, L. Liang, F. Wang, M. Liu, K. Chen, K. Sun, N. Zhang, J. Sun, Higher Yield Urea-Derived Polymeric Graphitic Carbon Nitride with Mesoporous Structure and Superior Visible-Light-Responsive Activity, ACS Sustain. Chem. Eng. 3 (2015) 3412–3419.

[38] L.A. Romero-Cano, H. Garcia-Rosero, F. Carrasco-Marín, A.F. Pérez-Cardenas, L.V. González-Gutiérrez, A.I. Zárate-Guzmán, G. Ramos-Sánchez, Surface functionalization to abate the irreversible capacity of hard carbons derived from grapefruit peels for sodium-ion batteries, Electrochim. Acta. 326 (2019) 134973.

[39] N. Chidhambaram, K. Ravichandran, Single step transformation of urea into metal-free g-C3N4 nanoflakes for visible light photocatalytic applications, Mater. Lett. 207 (2017) 44–48.

[40] S. Biniak, G. Szymański, J. Siedlewski, A. Świątkowski, The characterization of activated carbons with oxygen and nitrogen surface groups, Carbon N. Y. 35 (1997) 1799–1810.

[41] J.R. Pels, F. Kapteijn, J.A. Moulijn, Q. Zhu, K.M. Thomas, Evolution of nitrogen functionalities in carbonaceous materials during pyrolysis, Carbon N. Y. 33 (1995) 1641–1653.

[42] T. Sharifi, G. Hu, X. Jia, T. Wågberg, Formation of active sites for oxygen reduction reactions by transformation of nitrogen functionalities in nitrogen-doped carbon nanotubes, ACS Nano. 6 (2012) 8904–8912.

[43] T. Ikeda, M. Boero, S.-F. Huang, K. Terakura, M. Oshima, J.-I. Ozaki, Carbon Alloy Catalysts: Active Sites for Oxygen reduction Reaction, J. Phys. Chem. C. 112 (2008) 14706–14709.

[44] X. Bao, X. Nie, D. Von Deak, E.J. Biddinger, W. Luo, A. Asthagiri, U.S. Ozkan, C.M. Hadad, A first-principles study of the role of quaternary-N doping on the oxygen reduction reaction activity and selectivity of graphene edge sites, Top. Catal. 56 (2013) 1623–1633.

[45] Carrillo-Rodríguez, JC, Garay-Tapia AM, Escobar-Morales B, Escorcia-Garcia J, Ochoa-Lara MT, Rodríguez-Varela FJ, Alonso-Lemus IL. Insight into the performance and stability of Ndoped Ordered Mesoporous Carbon Hollow Spheres for the ORR: Influence of the nitrogen species on their catalytic activity after ADT. Int. J. Hydrog. Energy 2021;46;26087-100.

[46] Ferrero GA, Fuertes AB, Sevilla M, Titirici MM. Efficient metal-free N-doped mesoporous carbon catalysts for ORR by a template-free approach. Carbon 2016;106;179-87.

[47] Zhang J, Lv M, Lui D, Du L, Liang Z. Nitrogen-doped carbon nanoflower with superior ORR performance in both alkaline and acidic electrolyte and enhanced durability. Int. J. Hydrog, Energy 2018;43;4311-20.

[48] Tang J, Liu J, Li C, Li Y, Tade MO, Dai S, Yamauchi Y. Synthesis of nitrogen-doped mesoporous carbon spheres with extra-large pores through assembly of deblock copolymer micelles. Angew. Int. Ed. 2014;54;588-93.

[49] Liu J, Shan X, Wang G, Kong W. Meso-macroporous Carbons Decorated with Ample Nitrogen Sites as Bifunctional Catalysts in CO2 Catalytic Conversoin and Oxygen Reduction Reaction. ChemistrySelect 2021;6;1570-78.

[50] Cao R, Hu F, Zhang T, Shao W, Liu S, Jian X, Bottom-up fabrication of triazine-based frameworks as metal-free materialsfor supercapacitors and oxygen reduction reaction. RSC Adv. 2021;11;8384-93.

[51] Qi J, Jin B, Liu W, Zhang W, Xu L. Converting coals into carbon-based pH-universal oxygen reduction catalysts for fuel cells. Fuel 2021;285;119163.

[52] Chen P, Zang J, Zhou S, Jia S, Tian P, Cai H, Gao H, Wang Y. N-doped 3D porous carbon catalyst derived from biowaste Triarrhena sacchariflora panicle for oxygen reduction reaction. Carbon 2019;146;70-7.

[53] Cao Y, Liu Z, Tang Y, Wang Z, Liu F, Wen Y, Shan B, Chen R. Vaporized-salt-induced sp3 -hybridized defects on nitrogen-doped carbon surface towards oxygen reduction reaction. Carbon 2021;180;1-9.

[54] Quílez-Bermejo J, Gonzalez-Gaitán C, Morallón E, Cazorla-Amorós D, Effect of Carbonization Conditions of Polyaniline on Its Catalytic Activity towards ORR. Some Insights about the Nature of the Active Sites. Carbon 2017;119;62−71.

[55] Min J, Xu X, Koh J, Gong J, Chen X, Azadmanjiri J, Zhang F, Wen X, He C, Brachned Poly(L-lysine)-Derived Nitrogen-Containing Porous Carbon Flake as the Metal-Free Electrocatalyst towards Efficient Oxygen Reduction Reaction. ACS Appl. Energy Mater. 2021;4;3317-26.

[56] Begum H, Ahmed MS, Kim Y-B, Nitrogen-rich graphitic-carbon@graphene as a metal-free electrocatalyst for oxygen reduction reaction. Scient. Reports 2020;10;12431.

[57] Yang Y, He Z, Wang S, Wang H, Zhu G, Hyper-Crosslinked Polymer-Derived Nitrogen-Doped Hierarchical Porous Carbon as Metal-Free Electrocatalysts for High-Efficiency Oxygen Reduction. Energy Fuels 2021;23;19614-23.

[58] Ramírez-Pérez A., Quílez-Bermejo J, Sieben JM, Morallón E, Cazorla-Amorós D. Effect of Nitrogen-Functional Groups on the ORR Activity of Activated Carbon Fiber-Polypyrrole-Based Electrodes. Electrocatalysis 2018;9;697-705.

[59] Periyasamy G, Annamalai K, Patil IM, Kakade B. Sulfur and nitrogen co-doped rGO sheets as efficient electrocatalyst for oxygen reduction reaction in alkaline medium. Diam. Relat. Mater. 2021;114;108338.

[60] Pei Y, Song H, Liu Y, Cheng Y, Li W, Chen Y, Fan Y, Liu B., Lu S. Boron-nitrogen-doped carbon dots on multi-walled carbon nanotubes for efficient electrocatalysis of oxygen reduction reactions. J. Colloid Interface Sci. 2021;600;865-71.

[61] Ren S-B, Chen X-L, Li P-X, Hu D-Y, Liu H-L, Chen W, Xie W-B, Chen Y, Yang X-L, Han D-M, Ning G-H, Xia X-H. Nitrogen and sulfur dual-doped carbon nanotube derived from a thiazolothiazole based conjugated microporous polimer as efficient metal-free electrocatalysts for oxygen reduction reaction. J. Power Sources 2020;461;228145.

[62] Zhang H-J, Geng J, Cai C, Ma Z-F, Ma Z, Yao W, Yang J. Effect of doping order on metal-free heteroatoms dual-doped carbon as oxygen reduction electrocatalyst. Chin. Chem. Lett. 2021;32;745-9.

[63] Zheng B, Wang J, Pan Z, Wang X, Liu S, Ding S, Lang L, An efficient metal-free catalyst derived from waste lotus seedpod for oxygen reduction reaction. J. Porous Mater. 2020;27;637-46.

[64] Cao R, Hu F, Zhang T, Shao W, Liu S, Jian X, Botton-up fabrication of triazine-based frameworks as metal-free materials for supercapacitors and oxygen reduction reaction. RSC Adv. 2021;11;8384-93.

[65] Li D, Li C, Zhang L, Li H, Zhu L, Yang D, Fang Q, Qiu S, Yao X. Metal-Free Thiophene-Sulfur Covalent Organic Framework: Precise and Controllable Synthesis of Catalytic Active Sites for Oxygen Reduction. J. Am. Chem. Soc. 2020;142;8104-8.

[66] Lu H, Yang C, Chen J, Li J, Jin H, Wang J, Wang S. Tailoring Hierarchically Porous Nitrogen-, Sulfur-Codoped Carbon for High-Performance Supercapacitors and Oxygen Reduction. Small 2020;16;1906584.

[67] Wang Y, Xu N, He R, Peng L, Cai D, Qiao J, Large-scale defect-engineering tailored tri-doped graphene as a metal-free bifunctional catalyst for superior electrocatalytic oxygen reaction in rechargeable Zn-air battery. Appl. Catal. B 2021;285;119811.

[68] Zhou S, Zang J, Gao H, Tian X, Tian P, Song S, Wang Y. Deflagration method synthesizing N, S co-doped oxygen-functionalized carbons as a bifunctional catalyst for oxygen reduction and oxygen evolution reaction. Carbon 2021;181;234-45.

[69] Wang W, Wang P, Kang Y, Zhao J, Tao P, Lei Z, Flame synthesis of nitrogen, boron co-doped carbon as efficient electrocatalyst for oxygen reduction reaction. Int. J. Hydrog. 2019;44;4771-9.

[70] He Z, Wai P, Xu T, Han J, Gao X, Liu X. Defect-rich N/S-co-doped porous hollow carbon nanospheres derived from fullerenes as efficient electrocatalysts for the oxygen-reduction reaction and Zn-air batteries. Mater. Chem. Front. 2021;5;7873-82.

[71] Shen Y, Peng F, Cao Y, Zuo J, Wang H, Yu H. Preparation of nitrogen and sulfur co-doped ultrathin graphitic carbon via annealing bagasse lignin as potential electrocatalyst towards oxygen reduction reaction in alkaline and acid media. J. Energy Chem. 2019;34;33-42.

[72] Tuci G, Zafferoni ., Rossin A, Milella A, Luconi L, Innocenti M, Phuoc LT, Duong-Viet C, Pham-huu C, Giambastiani G. Chemically Functionalizated Carbon Nanotubes with Pyridines Groups as Easily Tunable N-decorated Nanomaterials for the Oxygen Reduction Reaction in Alkaline Medium. Chem. Mater. 2014;11;3460-70.

[73] Yasuda S, Yu L, Kim J, Murakoshi K., Selective nitrogen doping in graphene for oxygen reduction reactions. Chem. Comm. 2013;49;9627-9.

[74] Liu Y, He B, Qi C, Nitrogen-Doped Porous Graphene-like Carbon Nanosheets as Efficient Oxygen Reduction Reaction Catalysts under Alkaline and Acidic Conditions. Ind. Eng. Chem. Res. 2021;1;210-7.

[75] Li OL, Chiba S, Wada Y, Panomsuwan G, Ishizaki T, Synthesis of graphitic-N and amino-N in nitrogen-doped carbon via a solution plasma process and exploration of their synergic effect for advanced oxygen reduction reaction. J. Mater. Chem. A 20107;5;2073-82.

[76] Sun M, Wu X, Deng X, Zhang W, Xie Z, Huang Q, Huang B, Synthesis of pyridinic-N doped carbon nanofibers and its electro-catalytic activity for oxygen reduction reaction. Mater. Lett. 2018;220;313-6.

[77] Maouche C, Zhou Y, Li B, Cheng C, Wu Y, Li J, Gao S, Yang J. Thermal treated three-dimensional N-doped graphene as efficient metal free-catalyst for oxygen reduction reaction. J. Electroanal. Chem. 2019;853;113536.

[78] Wu X, Chen K, Lin Z, Zhang Y, Meng H. Nitrogen doped graphitic carbon from biomass as non noble metal catalysts for oxygen reduction reaction. Mater. Today 2019;13;100-8.

[79] Luo J, Wang K, Hua X, Wang W, Li J, Zhang S. Chen S., Pyridinic-N Protected Synthesis of 3D Nitrogen-Doped Porous Carbon with Increased Mesoporous Defects for Oxygen Reduction. Small 2019;15;1805325.

[80] Liu R, Wu D, Feng X, Müllen K, Nitrogen-Doped Ordered Mesoporous Graphitic Arrays with High Electrocatalytic Activity for Oxygen Reduction. Angewandte Chem. Int. 2010;49;2565-9.